Measurements of the effective electron density in an electron beam ion trap using extreme ultraviolet spectra and optical imaging

T. P. Arthanayaka, P. Beiersdorfer, G. V. Brown, M. Hahn, N. Hell, T. E. Lockard, and D. W. Savin

Citation: Review of Scientific Instruments **89**, 10E119 (2018); doi: 10.1063/1.5036758
View online: https://doi.org/10.1063/1.5036758
View Table of Contents: http://aip.scitation.org/toc/rsi/89/10
Published by the American Institute of Physics

Measurements of the effective electron density in an electron beam ion trap using extreme ultraviolet spectra and optical imaging

T. P. Arthanayaka,[1] P. Beiersdorfer,[2] G. V. Brown,[2] M. Hahn,[1] N. Hell,[2] T. E. Lockard,[2] and D. W. Savin[1,a)]
[1]*Columbia Astrophysics Laboratory, New York, New York 10027, USA*
[2]*Lawrence Livermore National Laboratory, Livermore, California 94550, USA*

(Presented 18 April 2018; received 18 April 2018; accepted 8 August 2018; published online 22 October 2018)

In an electron beam ion trap (EBIT), the ions are not confined to the electron beam, but rather oscillate in and out of the beam. As a result, the ions do not continuously experience the full density of the electron beam. To determine the effective electron density, $n_{e,eff}$, experienced by the ions, the electron beam size, the nominal electron density n_e, and the ion distribution around the beam, i.e., the so-called ion cloud, must be measured. We use imaging techniques in the extreme ultraviolet (EUV) and optical to determine these. The electron beam width is measured using $3d \rightarrow 3p$ emission from Fe XII and XIII between 185 and 205 Å. These transitions are fast and the EUV emission occurs only within the electron beam. The measured spatial emission profile and variable electron current yield a nominal electron density range of $n_e \sim 10^{11}$–10^{13} cm^{-3}. We determine the size of the ion cloud using optical emission from metastable levels of ions with radiative lifetimes longer than the ion orbital periods. The resulting emission maps out the spatial distribution of the ion cloud. We find a typical electron beam radius of ~60 μm and an ion cloud radius of ~300 μm. These yield a spatially averaged effective electron density, $n_{e,eff}$, experienced by the ions in EBIT spanning $\sim 5 \times 10^9$–5×10^{11} cm^{-3}. *Published by AIP Publishing.* https://doi.org/10.1063/1.5036758

I. INTRODUCTION

Electron density n_e is a fundamental parameter controlling the behavior of plasmas. Knowledge of n_e is needed for studies of astrophysical and laboratory plasmas. Spectroscopy is often used to measure n_e from ratios of emission line intensities, with at least one line being density sensitive. Essentially all such diagnostics are based on theoretical calculations for the relevant collisional excitation and de-excitation processes, radiative transition rates for the atomic levels involved, and cascade contributions from higher levels, but densities predicted using different atomic models can differ from one another by factors of up to an order of magnitude or more.[1] This limits our ability to understand and model the underlying physics of the observed plasmas.

To address this issue, we are benchmarking several spectroscopic density diagnostics, with an emphasis on Fe M-shell line intensity ratios relevant to solar physics. For this, we are using the Lawrence Livermore National Laboratory (LLNL) EBIT-I,[2–4] which enables us to study line ratios versus electron density. Such studies require reliable measurements of the effective electron density, $n_{e,eff}$, experienced by the ions in the device. The effective electron density accounts for the fact that the trapped ions spend a portion of their time outside the electron beam and thus do not see the full density contained in the beam.

To clarify, the effective density is not an issue for the observed dipole transitions commonly used for the density diagnostics. These dipole transitions can only be excited in the electron beam. Moreover, these levels decay so fast that the photon emission occurs only while the ions are in the beam. Rather, the issue relates to the ground and metastable levels out of which occurs the excitation to the dipole-allowed upper levels. The population of these lower levels is affected by the time that the ions spend outside the electron beam relative to the lifetime of the metastable level.

Here we describe how we measure the electron beam and ion cloud profiles in EBIT-I and derive $n_{e,eff}$. Section II describes the EBIT-I configuration. Section III discusses how we calculate the effective electron density. Section IV presents the imaging systems. Section V presents representative results. Section VI discusses our results.

II. EXPERIMENTAL OVERVIEW

EBIT-I is designed to study the interaction of highly charged ions with electrons by directly observing the emitted spectra. It has been described extensively elsewhere.[2–4] Here we discuss only those aspects of the device that are most relevant to the present results.

EBIT-I is a cylindrical trap with a 3 T axial magnetic field guiding a quasi-monoenergetic electron beam, running along the axis, and compressing it to a diameter of ~60 μm. The electron beam forms a negative potential well that radially confines positively charged ions. By varying the beam current, the nominal electron density can be varied[5] from

Note: Paper published as part of the Proceedings of the 22nd Topical Conference on High-Temperature Plasma Diagnostics, San Diego, California, April 2018.

a)Author to whom correspondence should be addressed: savin@astro.columbia.edu.

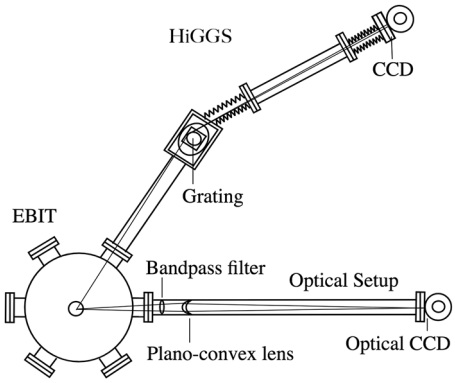

FIG. 1. Top-down schematic of the experimental setup. See the text for details.

$n_e \sim 10^{11}$ to 10^{13} cm^{-3}. Axial confinement is provided by a set of three drift tubes, the outer two of which are biased to form an ≈2 cm long trapping region for the ions.

Fe was introduced into EBIT-I as iron pentacarbonyl [$Fe(CO)_5$] using a collimated continuous ballistic gas injection system. The electron beam was used to dissociate the molecules, ionize the Fe up to the desired charge states, and then collisionally excite the trapped ions.

To determine $n_{e,eff}$, the electron beam current I_e, the electron beam size, and the ion cloud size must be measured. We use imaging techniques in the extreme ultraviolet (EUV) and optical, respectively, to determine these sizes. Figure 1 shows the portions of the EBIT-I setup that are most relevant to these measurements. The imaging systems are described in more detail in Sec. IV.

We floated the power supplies of the drift tubes to +345 V. The bottom drift tube was biased with an additional +520 V, the middle drift tube with an additional +50 V, and the top drift tube with an additional +450 V. The nominal electron beam energy in the trapping region was 395 eV. Accounting for the 5 mA beam current used here, the estimated space charge[6] was ≈40 V. Of this, typically half is cancelled by the charge of the trapped ions. This gives an electron beam energy of ≈375 ± 20 eV. The drift tube voltages created an axial trapping potential of +400 V.

The trapping cycle was 1 s long. At the end of each cycle, the trap was dumped for 5 ms by setting the additional voltage on the top drift tube to zero and turning off the electron beam. This prevented an accumulation of elements heavier than Fe, which come from the electron gun cathode and could contaminate the measured spectra.

Using this trapping cycle pattern, EUV and optical imaging data were accumulated for 30 min at a desired set of operating parameters. The imaging systems were ungated. Data were collected for the entire trapping cycle.

III. EFFECTIVE ELECTRON DENSITY

The geometrically averaged electron beam density n_e is

$$n_e = I_e \Big/ \pi r_e^2 e v_e. \quad (1)$$

Here I_e is the measured electron beam current, r_e is the average electron beam radius, e is the unit charge, and v_e is the velocity of the beam electrons. I_e is measured using an ammeter connected to the electron beam collector. The electron velocity is determined from the space-charge corrected beam energy. The electron beam radius is taken to be $r_e = \Gamma_e/2$, where Γ_e is the full width at half maximum (FWHM) of the electron beam. This approach assumes a uniform electron beam density.

The ions, however, experience an effective electron density $n_{e,eff}$ that is smaller than n_e, due to the oscillation of the trapped ions through the electron beam. The spatially averaged effective electron density $n_{e,eff}$ is given by[7]

$$n_{e,eff} = 4\ln(2) I_e \Big/ \pi\left(\Gamma_e^2 + \Gamma_i^2\right) e v_e. \quad (2)$$

Here Γ_i is the FWHM of the ion cloud. Hence, in order to determine $n_{e,eff}$, we need to measure both Γ_e and Γ_i.

IV. IMAGING SYSTEMS

A. EUV high resolution grating spectrometer

To determine the electron beam radius and, in turn, the nominal density, we used EBIT-I's high resolution grazing-incidence grating spectrometer (HiGGS) to measure Fe XII and Fe XIII EUV emission. The HiGGS uses a grating of 2400 lines/mm and a radius of curvature of R = 44.3 m. The dispersed emission was recorded with a liquid-nitrogen-cooled charge-coupled device (CCD). The spacing between the pixel centers on the CCD is 20 μm. The observed spectrum was centered on ~195 Å. Additional details of the HiGGS and the lines predicted in this range have been published previously.[8,9]

The collected EUV emission was generated by electron-impact excitation (EIE) of the trapped Fe ions. The resulting dipole-allowed radiative decays are fast, typically $\sim 5 \times 10^{10}$ s^{-1} for the Fe XII and XIII lines observed here.[10] This time scale is much shorter than the travel time of the ions through the electron beam. The ion temperature is $T_i \leq 10q$ eV, where q is the charge of the trapped ion.[11] For the ions considered here, $T_i \leq 140$ eV, resulting in a travel time of the ions through the electron beam of $\sim 2 \times 10^{-9}$ s. Hence, the EUV emission originates from within the electron beam, whose narrow diameter serves as an effective entrance slit for the spectrometer. No additional slit was needed.

Each spectral line thereby provides an image of the electron beam. The CCD position was varied to identify the optimal instrumental focus, to provide the most reliable electron beam diameter measurements. At the best focusing found in the 185–205 Å range, the spectrometer has a magnification of 1.00 ± 0.05. Here and throughout all uncertainties are quoted at a 1σ confidence level.

Additional contributions to the line widths are insignificant. The natural widths are much smaller than the line width due to the electron beam diameter. Doppler broadening from the ion motion in EBIT is also not significant. For the ions studied, $T_i \leq 140$ eV, corresponding to a line width of less than ~0.023 Å. This is smaller than the measured line widths of ~0.050 Å. Hence, the observed line width is primarily due to the electron beam diameter. Subtracting in quadrature, the

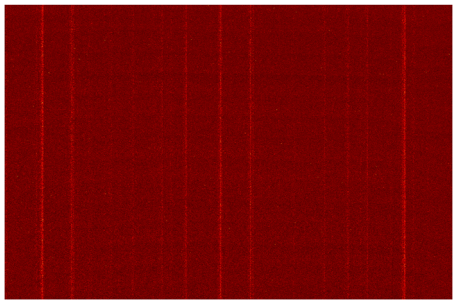

FIG. 2. CCD image of an HiGGS spectrum. The CCD image is 1280 pixels wide and 1240 pixels high. Each red dot corresponds to a photon and a higher density of red dots indicates more photons per area. The background is black. See the text for details.

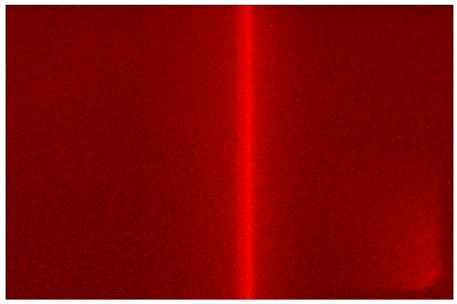

FIG. 4. Optical image of the ion cloud. This corrected CCD image is 1250 pixels wide and 1200 pixels high. Each red dot corresponds to a photon and a higher density of red dots indicates more photons per area. The background is black. See the text for details.

Doppler contribution to the line width reduces the measured beam diameter by less than ~10%.

A typical CCD image of an HiGGS spectrum is shown in Fig. 2. These data, collected using an electron beam of ≈375 eV and 5 mA, are primarily due to Fe XII and XIII. For data reduction, the image was first rotated by 1.1° to account for the slight misalignment between the electron beam and the vertical pixel columns in the CCD. The edges of the CCD image were then cropped so that the new edges were perpendicular and parallel to the imaged spectral lines. Next, cosmic rays were removed. Finally, the background was subtracted out, yielding images such as in Fig. 2.

Spectra are generated by collapsing the corrected CCD images onto the horizontal axis (Fig. 3). In Sec. V, we discuss how we fit the measured line shapes in such spectra in order to determine the electron beam diameter.

B. Optical system

The visible light imaging system is similar to that used previously on EBIT-I.[12,13] The first element is a bandpass filter centered at 530 nm with a bandwidth of 10 nm. This eliminates most of the visible light from fast transitions in background atoms and ions. It also eliminates much of the stray light due to the glow of the electron beam cathode. The filter is followed by a plano-convex lens with a focal length of 50.1 ± 0.5 cm and then a liquid-nitrogen-cooled CCD. The spacing between the pixel centers on the CCD is 20 μm. The magnification of the setup is 3.05 ± 0.06.

The optical system was used to monitor EIE emission from metastable levels in Fe XIV. The line observed was the $3s^2 3p(^2P_{3/2}) \rightarrow 3s^2 3p(^2P_{1/2})$ transition at 530.29 nm. The radiative lifetime of the upper level in this transition is 16.7 ms.[14,15] The ions are excited within the electron beam. But the long lifetime of this metastable level results in the ions radiatively relaxing randomly along their orbits. Hence, the observed emission spans the stored ion cloud and provides a measure of the spatial distribution of the trapped ions.

In order to accurately determine the effective electron density experienced by the trapped ions, it is preferable to measure both the electron beam and ion cloud profiles using the charge state of interest. We plan to benchmark for solar physics several commonly used Fe XII and XIII electron density diagnostics. Hence, it would have been preferable to measure the ion cloud using the metastable Fe XII $3s^2 3p^3(^2P^o_{1/2}) \rightarrow 3s^2 3p^3(^2D^o_{3/2})$ line at 307.20 nm and the Fe XIII $3s^2 3p^2(^1D_2) \rightarrow 3s^2 3p^2(^3P_2)$ line at 338.81 nm. But these two lines were too weak to detect. Fortunately, given the small difference in charge state between Fe XII, XIII, and XIV, we expect the ion clouds for Fe XII and XIII to be nearly identical to that measured for Fe XIV.[16]

A typical optical image of the trapping region is shown in Fig. 4. These data were collected simultaneously with those

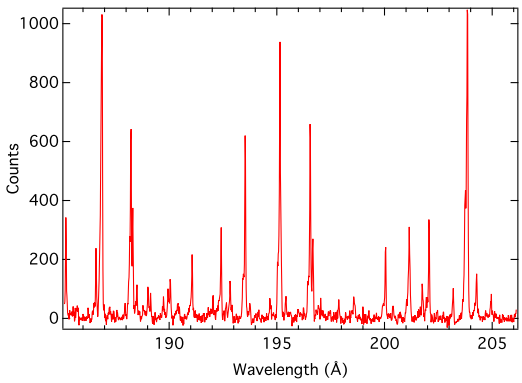

FIG. 3. HiGGS spectrum generated from Fig. 2. See the text for details.

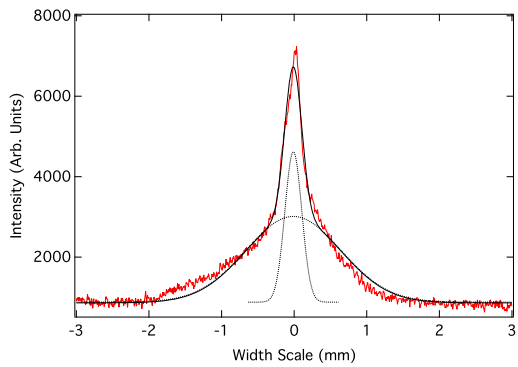

FIG. 5. Optical image of the ion cloud, generated from Fig. 4. The width scale is in the object plane. The red curve shows the data, the black line gives the fit, and the dotted black lines shows the two Gaussian components. See the text for details.

shown in Figs. 2 and 3 and reduced using the same processes (cosmic ray removal, background subtraction, rotation by 0.5°, and cropping), as described above.

Line outs of the ion cloud images were generated by collapsing the corrected CCD images onto the horizontal axis (Fig. 5). Here we used only the top half of Fig. 4 to avoid the effects of the elevated background in the lower right-hand corner of Fig. 4. We attribute this elevated background to light reflecting off of the middle drift tube. In Sec. V B, we discuss how we fit the imaged cloud in order to determine the distribution of the ions.

V. RESULTS

A. Electron beam diameter

An EUV lineout of the electron beam is shown in Fig. 6, extracted from the spectrum shown in Fig. 2. The width scale on the x axis is calculated using the CCD pixel spacing and the magnification of the system.

The Fe XII $3s^2 3p^2(^3P)3d(^4P_{5/2}) \rightarrow 3s^2 3p^3(^4S^o{}_{3/2})$ transition at 195.12 Å is the strongest line. On the long wavelength side is the $3s^2 3p^2(^1D)3d(^2D_{5/2}) \rightarrow 3s^2 3p^3(^2D_{3/2})$ transition in Fe XII at 195.18 Å. Two weak lines at 195.00 and 195.05 Å are unidentified. We fit the four lines using Gaussian shapes, with the widths of all the four linked together. The resulting FWHM was found to be $\Gamma_e = 58.0 \pm 4.8$ μm. This is in good agreement with previous LLNL measurements using a slit to image the beam in X-rays.[17,18]

B. Ion cloud size

The ion cloud image in Fig. 5 is broad and asymmetric. The FWHM is 354 μm, but the shape suggests that there are multiple components and that this FWHM is unlikely that of the Fe XIV cloud. So we have approximated the image using two Gaussians with different widths. Figure 5 shows our fit. We find a narrow Gaussian base with a FWHM of $\Gamma_{i,n} = 278 \pm 3$ μm and of a broad Gaussian base with a FWHM of $\Gamma_{i,w} = 1544 \pm 16$ μm.

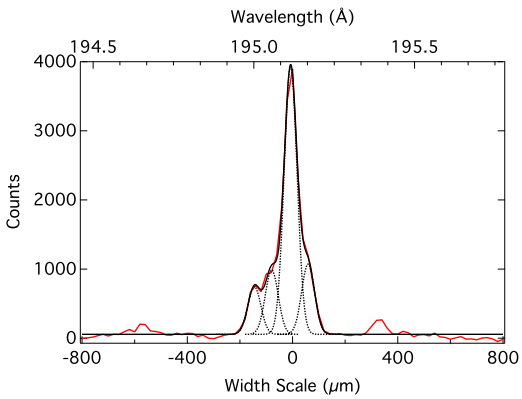

FIG. 6. EUV image of the electron beam from the HiGGS results in Fig. 3. The red line is the measured intensity, the black line is the fit to the observed features, and the four dotted black lines are the individual Gaussian line profiles making up the fit. The width scale in the object plane is shown on the bottom axis and the wavelength scale on the top axis. See the text for details.

We attribute the narrow Gaussian to metastable Fe XIV emission and the asymmetry and broader base, in part, to aberrations in the lens as well as a slight misalignment of the lens plane relative to the object plane. We independently tested the optical system by imaging a slit of width 216 ± 13 μm. The resulting image could be well fit using a narrow Gaussian with a FWHM of ≈200 ± 20 μm and a broader Gaussian with a FWHM between ~500 and 800 μm and with a centroid that shifted relative to that of the narrow Gaussian as the lens plane was adjusted. The good agreement between the width of the narrow Gaussian and the slit width gives us confidence that the aberrations and misalignments in the optical system have less than a 10% effect on the measured ion cloud width.

Additional contributions to the asymmetry and broad base of the image may be due to reflection from the drift tube and emission from metastable levels in Fe III, VI, and VII. These three ions have metastable levels that emit within the bandpass of our optical filter.[10] Although the ionization energy of these ions is lower than that for Fe XIV formation, the continuous gas injection results in a constantly replenishing population of charge states significantly below Fe XIV. These lower charged ions are less strongly bound in the trap than Fe XIV. As a result, their orbits may be wider than the more strongly trapped Fe XIV.

C. Effective electron density

The nominal value of n_e is given by Eq. (1). For the Fe XII data shown earlier, we find $n_e \approx 1.0 \times 10^{12}$ cm^{-3}. The ions, however, experience an effective electron density $n_{e,eff}$ that is smaller than n_e. The spatially averaged effective electron density $n_{e,eff}$ is given by Eq. (2), where we set $\Gamma_i = \Gamma_{i,n}$. This yields $n_{e,eff} = 3.0 \times 10^{10}$ cm^{-3}.

The quantity that we actually need in order to benchmark spectroscopic electron density diagnostics is the time-average effective electron density experienced by the ions in the trap. We plan in the near future to computationally simulate the ion trajectories in EBIT-I and determine the relationship between the spatially and time-averaged effective electron densities.

VI. DISCUSSION

Our results here provide an important exploration of potential systematic issues related to electron beam and ion cloud measurements in an EBIT. Earlier measurements have been reported using a compact EBIT (CoBIT),[7] but with different operating conditions and diagnostics. For instance, the magnetic field in CoBIT is 0.2 T, compared to our 3 T. As a result the electron beam and ion cloud diameters are ~4 times larger in CoBIT than in EBIT-I. To measure their electron beam diameter, the CoBIT group used an EUV pinhole camera and found the beam shape to be asymmetric. They attribute this to a misalignment of the magnetic field and drift tubes in CoBIT. Here we use EUV spectroscopy and find the beam to be symmetric in shape, supporting their suggestion of a misaligned machine. For the ions, the CoBIT group measured the cloud shape using visual spectroscopy, observing a specific transition in Fe XI. Here we use a narrow-band filter centered on a specific transition in Fe XIV. Their measurements and ours both found that the ion cloud is asymmetric and that

the image sits on top of a broad background that is not flat. In our case, these issues are likely due to optical aberrations and misalignment.

Typical EBIT-I operating conditions generate nominal densities of $n_e \sim 10^{11}$–10^{13} cm^{-3}. Based on our measured electron beam and ion cloud diameters, we expect to be able to generate spatially averaged effective electron densities of $n_{e,\mathrm{eff}} \sim 5 \times 10^9$ to 5×10^{11} cm^{-3}, which are typical of the solar corona.[1] EBIT-I is thus well poised to study many electron density diagnostics relevant to coronal physics studies.

ACKNOWLEDGMENTS

This work was supported in part by NASA H-TIDeS Grant No. NNX16AF10G. Work at LLNL is performed under the auspices of the U.S. DoE under Contract No. DE-AC52-07NA27344.

[1]P. R. Young, T. Watanabe, H. Hara, and J. T. Mariska, Astron. Astrophys. **495**, 587 (2009).
[2]M. A. Levine, R. E. Marrs, J. N. Bardsley, P. Beiersdorfer, C. L. Bennett, M. H. Chen, T. Cowan, D. Dietrich, J. R. Henderson, D. A. Knapp *et al.*, Nucl. Instrum. Methods Phys. Res., Sect. B **43**, 431 (1989).
[3]R. E. Marrs, P. Beiersdorfer, and D. Schneider, Phys. Today **47**(10), 27 (1994).
[4]P. Beiersdorfer, Can. J. Phys. **86**, 1 (2008).
[5]H. Chen, P. Beiersdorfer, L. A. Heeter, D. A. Liedahl, K. L. Naranjo-Rivera, and E. Träbert, Astrophys. J. **611**, 598 (2004).
[6]D. Vogel, Lawrence Livermore National Laboratory Internal Report No. UCRL-ID-104990, 1990.
[7]E. Shimizu, S. Ali, T. Tsuda, H. A. Sakaue, D. Kato, I. Murakami, H. Hara, T. Watanabe, and N. Nakamura, Astron. Astrophys. **601**, A111 (2017).
[8]P. Beiersdorfer, E. W. Magee, G. V. Brown, N. Hell, E. Träbert, and K. Widmann, Rev. Sci. Instrum. **85**, 11E422 (2014).
[9]P. Beiersdorfer, E. Träbert, J. K. Lepson, N. S. Brickhouse, and L. Golub, Astrophys. J. **788**, 25 (2014).
[10]A. Kramida, Yu. Ralchenko, J. Reader, and NIST ASD Team, *NIST Atomic Spectra Database* (National Institute of Standards and Technology, Gaithersburg, MD, 2018), verision 5.5.2 [Online], available: https://physics/nist.gov/ads; 13 March 2018.
[11]P. Beiersdorfer, V. Decaux, S. R. Elliott, K. Widmann, and K. Wong, Rev. Sci. Instrum. **66**, 303 (1995).
[12]J. R. C. López-Urrutia, P. Beiersdorfer, K. Widmann, and V. Decaux, Phys. Scr. **T80**(B) 448 (1999).
[13]E. Träbert and P. Beiersdorfer, Rev. Sci. Instrum. **74**, 2127 (2003).
[14]P. Beiersdorfer, E. Träbert, and E. H. Pinnington, Astrophys. J. **587**, 836 (2003).
[15]G. Brenner, J. R. C. López-Urrutia, Z. Harman, P. H. Mokler, and J. Ullrich, Phys. Rev. A **75**, 032504 (2007).
[16]G. Y. Liang, J. R. C. López-Urrutia, T. M. Baumann, S. W. Epp, A. Gonchar, A. Lapierre, P. H. Mokler, M. C. Simon, H. Tawara, V. Mäckel, K. Yao, G. Zhao, Y. Zou, and J. Ullrich, Astrophys. J. **702**, 838 (2009).
[17]R. E. Marrs, P. Beiersdorfer, S. R. Elliott, D. A. Knapp, and Th. Stoekhler, Phys. Scr. **T59**, 183 (1995).
[18]S. B. Utter, P. Beiersdorfer, J. R. Crespo López-Urrutia, and K. Widmann, Nucl. Instrum. Meth. Phys. Res., Sect. A **428**, 276 (1999).